Electrophysiological Alterations of Pyramidal Cells and Interneurons of the CA1 Region of the Hippocampus in a Novel Mouse Model of Dravet Syndrome

David A. Dyment,*,† Sarah C. Schock,† Kristen Deloughery,† Minh Hieu Tran,† Kerstin Ure,‡ Lauryl M. J. Nutter,§ Amie Creighton,§ Julie Yuan,§ Umberto Banderali, Tanya Comas,** Ewa Baumann,** Anna Jezierski,** Care4Rare Canada Consortium,* Kym M. Boycott,*,† Alex E. Mackenzie,* and Marzia Martina****

*Children's Hospital of Eastern Ontario Research Institute, and †Department of Genetics, Children's Hospital of Eastern Ontario, Ottawa, K1H 8L1 Ontario, Canada, ‡Behaviour and Physiology Core, University of Ottawa, K19 6N5 Ontario, Canada, §The Centre for Phenogenomics, The Hospital for Sick Children, Toronto, M5T 3H7, Ontario, Canada, and **National Research Council of Canada, Human Health Therapeutics Research Center, Ottawa, K1A 0R6 Ontario, Canada

ABSTRACT Dravet syndrome is a developmental epileptic encephalopathy caused by pathogenic variation in *SCN1A*. To characterize the pathogenic substitution (p.H939R) of a local individual with Dravet syndrome, fibroblast cells from the individual were reprogrammed to pluripotent stem cells and differentiated into neurons. Sodium currents of these neurons were compared with healthy control induced neurons. A novel *Scn1a*$^{H939R/+}$ mouse model was generated with the p.H939R substitution. Immunohistochemistry and electrophysiological experiments were performed on hippocampal slices of *Scn1a*$^{H939R/+}$ mice. We found that the sodium currents recorded in the proband-induced neurons were significantly smaller and slower compared to wild type (WT). The resting membrane potential and spike amplitude were significantly depolarized in the proband-induced neurons. Similar differences in resting membrane potential and spike amplitude were observed in the interneurons of the hippocampus of *Scn1a*$^{H939R/+}$ mice. The *Scn1a*$^{H939R/+}$ mice showed the characteristic features of a Dravet-like phenotype: increased mortality and both spontaneous and heat-induced seizures. Immunohistochemistry showed a reduction in amount of parvalbumin and vesicular acetylcholine transporter in the hippocampus of *Scn1a*$^{H939R/+}$ compared to WT mice. Overall, these results underline hyper-excitability of the hippocampal CA1 circuit of this novel mouse model of Dravet syndrome which, under certain conditions, such as temperature, can trigger seizure activity. This hyper-excitability is due to the altered electrophysiological properties of pyramidal neurons and interneurons which are caused by the dysfunction of the sodium channel bearing the p.H939R substitution. This novel Dravet syndrome model also highlights the reduction in acetylcholine and the contribution of pyramidal cells, in addition to interneurons, to network hyper-excitability.

KEYWORDS Dravet syndrome; induced neurons; pyramidal cells; interneurons; CA1; hippocampus; sodium current; mouse model

DRAVET syndrome (DS) is an early-onset infantile epileptic encephalopathy in which pathogenic variation in *SCN1A*, encoding the α1 subunit of the voltage-gated sodium channel ($Na_v1.1$), is responsible. The pathogenic variant is detectable in 70–80% of individuals with the clinical diagnosis of DS (Claes *et al.* 2001; Hirose *et al.* 2013). An infant typically presents at 6 months of age with febrile seizures that evolve to include status epilepticus, myoclonic, focal, and generalized seizures that are refractory to treatment (Dravet 2011).

Animal models have provided important insights into the underlying mechanism of DS (Oakley *et al.* 2011). Knockout mouse models have been generated that faithfully recapitulate the DS phenotype as the mice show severe, temperature-sensitive seizures and increased mortality (Yu *et al.* 2006; Ogiwara *et al.* 2007). Reduced excitability of GABAergic

doi: https://doi.org/10.1534/genetics.120.303399
Manuscript received March 27, 2020; accepted for publication June 5, 2020; published Early Online June 17, 2020.
Supplemental material available at figshare: https://doi.org/10.25386/genetics.12475901.
[1]Corresponding author: Children's Hospital of Eastern Ontario Research Institute, 401 Smyth Rd., Ottawa, ON, Canada. E-mail: ddyment@cheo.on.ca

interneurons has been shown (Yu *et al.* 2006), and, when the channel is conditionally knocked out in GABAergic interneurons of the cortex, the mutation is sufficient to cause the disease (Cheah *et al.* 2012; Ogiwara *et al.* 2013). Given these observations, DS has been described as an "interneuronopathy" (Catterall 2018).

To gain further insight into the pathophysiology of the DS, we generated a novel mouse model based on an amino acid substitution in $Na_v1.1$ (p.H939R), modeled on a local patient with DS. To investigate the neuronal network causing the seizures, immunohistochemistry and electrophysiological experiments were performed on hippocampal slices of these mice. In addition, fibroblasts from the proband were reprogrammed into induced pluripotent stem cells (iPSCs) and then differentiated to mixed forebrain neurons (iNs). These iNs were then studied using whole-cell patch-clamp.

Materials and Methods

Generation of induced pluripotent stem cells (iPSCs) from primary patient fibroblasts derived from proband

All media and kits were purchased from Stemcell Technologies (Vancouver, BC, Canada). To convert patient fibroblasts to iPSCs (DS-iPSCs), the OKSGM kit was used in accordance with the manufacturer's instructions. Briefly, fibroblasts were plated onto Matrigel Basement Membrane Matrix (Corning; Tewkesbury, MA) and transfected with ReproRNA-OKSGM cocktail. Puromycin selection was carried out 1 day after transfection. iPSC colonies were picked between 18 and 28 days after transfection and maintained in Matrigel Basement Membrane Matrix and mTeSR1 for expansion. Wild-type (WT) iPSCs from healthy donors (WT-iPSCs) were used as previously described (Ribecco-Lutkiewicz *et al.* 2018).

Differentiation of iPSCs into mixed forebrain neurons

To generate neurons (iNs), iPSCs were dissociated using ReLeSR passaging reagent and passaged at a 1:6 ratio onto Matrigel coated plates in STEMdiff Neural Induction Medium (Stemcell Technologies). Media was changed daily, as per manufacturer's protocols for monolayer differentiation. Neural progenitors were dissociated using Accutase, according to the manufacturer's instructions, and then subcultured. After 3 weeks in neural induction media, the neuronal progenitor cells were replated and expanded in STEMdiff Neural Progenitor medium (Stemcell Technologies), which was replenished daily. To induce neuronal differentiation, the media was switched to STEMdiff neuron maturation kit (Stemcell Technologies), used according to the manufacturer's instructions, to generate a mixed population of excitatory and inhibitory forebrain type neurons. Final maturation of the neurons was in BrainPhys media (Stemcell Technologies) supplemented with 20 ng/ml glial derived neurotrophic factor (GDNF), 20 ng/ml brain derived neurotrophic factor (BDNF), 1 mM dibutyryl cyclic AMP (db-cAMP), and 200 nM ascorbic acid. The neurons were plated on plastic coverslips coated with Matrigel and kept in an incubator at 37° and 5% CO_2 and allowed to mature for at least 45 days before the electrophysiological recordings.

Animals

The *Scn1a* mutant mice were generated by direct delivery of Cas9 reagents to C57BL/6NCrl (Strain 027; Charles River Laboratories, Wilmington, MA) mouse zygotes, at The Centre for Phenogenomics (Toronto, ON, Canada) (Gertsenstein and Nutter 2018). Briefly, a single guide RNA with the desired spacer sequence (see Supplemental Material, Materials and Methods S1) was synthesized by *in vitro* transcription from a PCR-derived template. A microinjection mix of 30 ng/μl Cas9 protein (PNA Bio CP01-50) precomplexed with 20 ng/μl gRNA and 10 ng/μl single-strand oligonucleotide template (see *Materials and Methods* S1, mutated nucleotides indicated in lowercase) was microinjected into C57BL/6NCrl zygotes. Injected zygotes were incubated in $KSOM^{AA}$ media (ZEKS-50; Zenith Biotech) at 37° with 6% CO_2 until same-day transfer into CD-1 (Strain 022; Charles River Laboratories) surrogate host mothers. PCR primers flanking the sgRNA target site (*Scn1a* primers, see Materials and Methods S1) and outside of the repair template homology arms, were used to amplify the region of interest from founder progeny. PCR amplicons were subjected to Sanger sequencing. Founders with the desired nucleotide changes were selected for breeding with C57BL/6NCrl mice to produce N1 progeny that were confirmed by sequence analysis of PCR amplicons using the same PCR primers as for founder screening.

Colony

All experiments conformed to the guidelines set forth by the Canadian Council for the Use and Care of Animals in Research (CCAC), with approval from the University of Ottawa Animal Care Facility. $Scn1a^{H939R/+}$ male mice showed reduced fertility, similar to observations from another group studying *Scn1a* deletion on a C57BL/6 background.[13] Females showed a reduced fertility as well as a reduction in the number of offspring compared to control females. As such, *in vitro* fertilization was used to maintain the colony. For this, sperm was collected from the epididymis of >8-week-old heterozygous males for *in vitro* fertilization of oocytes collected from super-ovulated 3- to 4-week-old C57BL/6NCrl females. After 4 hr of co-incubation, embryos were washed to remove excess sperm and incubated overnight at 37° and 5%CO_2:5%O_2:90% N_2. Two-cell embryos were transferred into pseudopregnant CD-1 females for gestation and birth. Pups were genotyped after weaning at 3 weeks of age using a real-time PCR allelic discrimination assay. Offspring showed a Mendelian ratio of DS *vs.* WT births, and male *vs.* females born. For experiments, male and female mice that were N3 or greater backcrosses were used. Mice were weighed every week for a total of 10 weeks.

Phenotyping box

Seizures were visualized using Noldus PhenoTyper boxes (Noldus Information Technology, Wageningen, The Netherlands). Female and male mice were individually housed in

these cages on a 7 AM–7 PM regular light cycle with free access to food and water as well as a nest box. Mice were recorded for 1 day at ambient room temperature and a second day at 30°. To increase the temperature to 30°, space heaters were used in the room. Seizures were assessed by blinded manual analysis and were scored on character and frequency. The seizure categories were based on a revised Racine scale. For this scale, "one to two" were not recorded, "three to four" were grouped as "mild" severity, "five" was grouped as "medium" severity, and "six" as "severe" seizures.

Electrophysiological recordings

Preparation of hippocampal slices: Coronal brain slices containing the hippocampus were obtained from female and male 8-week-old *Scn1a*$^{H939R/+}$ and WT mice. Prior to decapitation, animals were anesthetized with isoflurane (4%, 2 liter/min O_2 flow rate). The brain was removed and placed in an oxygenated (95% O_2/5% CO_2) physiological solution, artificial cerebrospinal fluid (ACSF), at 4° Containing (mM) 126 NaCl, 2.5 KCl, 1 $MgCl_2$, 26 $NaHCO_3$, 1.25 NaH_2PO_4, 2 $CaCl_2$, and 10 glucose (300 mOsm, pH = 7.2). A tissue block containing the hippocampal region of interest was sectioned into 300 μm thick slices using a vibrating microtome (VT 1200S; Leica, Buffalo Grove, IL). Slices were incubated in an oxygenated submersion chamber at room temperature prior to recording. One slice was then transferred to a recording chamber (submerged type) perfused with oxygenated ACSF (2 ml/min).

Patch-clamp recordings in current-clamp mode: Whole-cell patch-clamp recordings in current-clamp mode were performed at room temperature using borosilicate pipettes filled with a pipette solution containing (in millimolar) 130 K^+-gluconate, 10 N-2-hydroxy-ethylpiperazine-N′-2-ethanesulfonic acid (HEPES), 10 KCl, 2 $MgCl_2$, 0.5 ethylene glycol-bis (β-aminoethyl ether)-N,N,N′,N′-tetraacetic acid (EGTA), 4 ATP-Mg, 0.2 GTP. The pH was adjusted to 7.2 with CsOH and osmolarity to 280–290 mOsm. Pipettes had a resistance of 3–5 MΩ when filled with the above solution. Whole-cell access resistance ranged from 5 to 15 MΩ and was monitored throughout the experiments.

Whole-cell patch-clamp recordings were obtained with a Multiclamp 700B amplifier (Molecular Devices, San Jose, CA) controlled with a pClamp 10 software (Molecular Devices) used in combination with a Digidata 1320A A/D converter (Molecular Devices). Data were acquired at 20 kHz and filtered at 2 kHz.

iNs derived from DS-iPSCs (see above) and WT-iNs were plated on plastic coverslips. The coverslips were inserted into a perfusion chamber (Warner Instruments, Hamden, CT) under a biologic hood. The chamber was then transferred under an inverted microscope (Nikon Eclipse TI; Nikon Instruments, Melville, NY) for patch-clamp experiments. The cells were recorded in ACSF solution (see above) at room temperature.

Cells in brain slices were patched under visual control using differential interference contrast and infrared video microscopy (IR-DIC; Olympus BX50WI; Olympus Canada, Markham, ON, Canada). Data were analyzed using pClamp10 (Molecular Devices). Statistical significance of the results was determined with Student's *t*–tests (two-tailed). All values are expressed as means ± SEM, and a *P*-value of <0.05 was considered significant. Whole-cell currents were recorded from individual pyramidal cells and interneurons voltage-clamped at resting membrane potentials. Recordings were obtained from pyramidal neurons and interneurons in the stratum pyramidale and stratum radiatum of the CA1 region of the hippocampus, respectively. We recorded from interneurons located ~250–300 μm from the stratum pyramidale. Following the interneuron classification (Klausberger 2009), we suggest that the interneurons we recorded were Schaffer collateral-associated cells and/or apical dendrite innervating cells, which express cholecystokinin (*i.e.*, CCK-expressing interneurons) (Klausberger 2009). The soma of Schaffer collateral-associated cells is located mainly in stratum radiatum with dendrites spanning all layers. The axons of these cells innervate the oblique and, to a lesser extent, basal dendrites of CA1 pyramidal neurons and interneurons mainly in stratum radiatum (Klausberger 2009). Apical dendrite innervating cells have soma, dendritic, and axonal distributions very similar to those of Schaffer collateral-associated cells. However, electron microscopic investigations have indicated that the apical dendrite-targeting cells innervate preferentially the main apical shaft of CA1 pyramidal neurons (Klausberger *et al.* 2005).

The electro-responsive properties of neurons (pyramidal cells and interneurons in slices) and iNs were studied in current-clamp by applying current pulses from resting membrane voltage (V_m) in ACSF. The amplitude of current pulses was varied in increments of 10 pA (or otherwise mentioned in the text). The input resistance (R_{in}) was estimated in the linear portion of current–voltage plots. The membrane time-constant (τ) was derived from single exponential fits to voltage responses. The spike amplitude and the spike duration at half-amplitude were measured from the first action potential evoked by a current pulse. The spike amplitude was measured from the spike threshold to the peak (overshoot of the spike). The spike duration half amplitude was measured in milliseconds at the 50% of the spike amplitude after the spike amplitude was established.

Patch-clamp recordings in voltage-clamp mode: Whole-cell patch-clamp recordings in voltage-clamp mode were performed at room temperature using borosilicate pipettes filled with a pipette solution containing (in millimolar): 140 Cs^+-fluoride, 10 NaCl, 1 EGTA, 10 HEPES. The pH was adjusted to 7.3 with CsOH and osmolarity to 280–290 mOsm. Pipettes had a resistance of 3–5 MΩ when filled with the above solution. Whole-cell access resistance ranged from 5 to 15 MΩ and was monitored throughout the experiments. Series resistance was corrected at 60–70%. The bath solution was normal ACSF (see above). Whole-cell patch-clamp recordings and analysis were obtained as described above. The time constant (τ) of the recovery from inactivation was obtained by fitting to a single exponential the averaged time

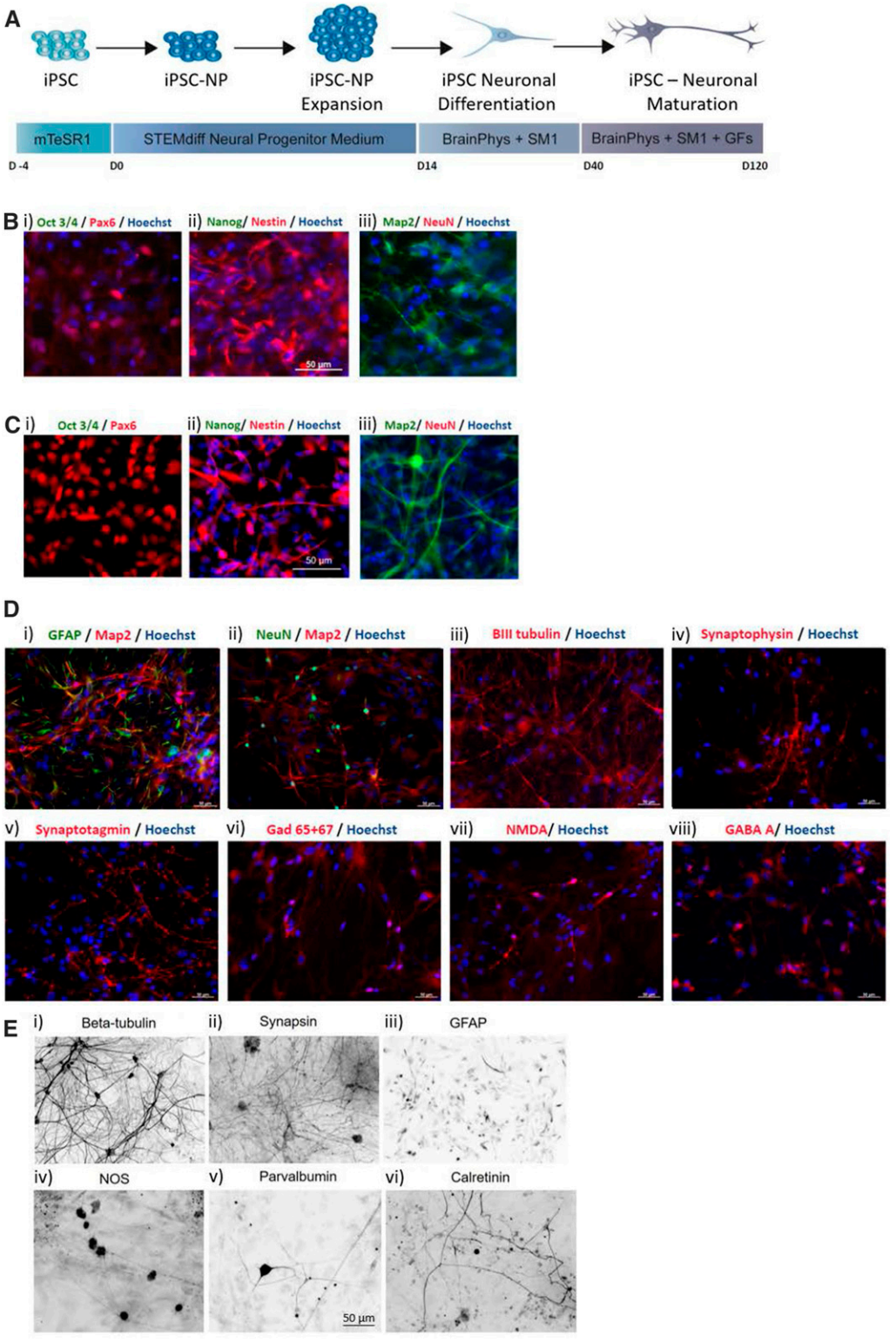

Figure 1 Characterization of iPSC-derived control and Dravet neurons. (A) Schematic detailing timeline for iPSC differentiation toward neural progenitors (iNPCs) and mature neurons (iNs). (B) Immunofluorescence images of control iPSC-derived neural progenitors expressing (i) Pax6, (ii) Nestin and (iii) Map2 and negative for the expression of pluripotency markers (i) Oct3/4 and (ii) NANOG and (iii) mature neuronal marker NeuN. (C) Immunofluorescence images of Dravet iPSC-derived neural progenitors expressing (i) Pax6, (ii) Nestin, and (iii) Map2 and negative for the expression of pluripotency markers (i) Oct3/4, and (ii) NANOG and (iii) mature neuronal marker NeuN. (D) Immunofluorescence staining in control induced neurons for several neuronal markers including (i) and (ii) Map2, (iii) βIII-tubulin, (ii) NeuN; synaptic proteins, (iv) Synaptophysin, (v) Synaptotagmin; and receptors expressed in mature iNs (vi) GAD 65+67, (vii) NMDA, and (viii) GABA. Astrocytes express GFAP (i) Hoescht was used as the nuclear counterstain. (E) Inverted immunofluorescence images of Dravet-induced neurons expressing the neuronal marker (i) βIII-tubulin, (ii) the synaptic marker synapsin, (iii) the glial marker GFAP, and (iv) interneuronal markers nitric oxide synthase (NOS), (v) Parvalbumin and (vi) Calretinin. All scale bars provided in (B–E) represent 50 µm.

courses of the current recovery. The time course of current recovery was calculated comparing the peak currents between a prepulse (0 mV) and a test voltage pulse (0 mV) separated by intervals of increasing durations (0.5 msec increments) at −120 mV (Figure 2D).

Na^+ conductance (G_{Na}) was calculated by dividing the amplitude of the current (I) recorded at a given voltage by the voltage amplitude (V) corrected for the Na^+ Nernst potential (+69.6 mV), in the voltage region of the sigmoidal G_{Na}/V relationship where G_{Na} is maximum (G_{max}, see Equation 1). For

Table 1 Properties of Na^+ currents in WT-iNs and DS-iNs

	WT-iNs	DS-iNs
Peak current amplitude (pA)	7516 ± 2199 (n = 8)	1997 ± 507* (n = 26)
Voltage peak current (mV)	−16.4 ± 5.2 (n = 7)	−5.6 ± 2.8 (n = 26)
Activation τ (msec)	0.51 ± 0.11 (n = 7)	1.63 ± 0.38* (n = 24)
Inactivation τ (msec)	1.15 ± 0.16 (n = 6)	1.51 ± 0.16 (n = 20)
G/G_{max} half (mV)	−28.3 ± 4.6 (n = 7)	−21.4 ± 2.3 (n = 26)
I/I_{max} half (mV)	−53.3 ± 1.7 (n = 6)	−56.8 ± 3.0 (n = 21)
Recovery from inactivation (msec)	1.73 ± 0.12 (n = 7)	1.84 ± 0.16 (n = 18)
Persistent current (% of peak)	0	11.04 ± 3.49 (n = 10)
Percentage of cells with persistent current (%)	0	38.5%

* $p < 0.05$.

a more accurate comparison of the Na^+ conduction properties of the membranes of WT- and DS-iNs neurons, we compared the conductance densities (expressed in nS/pF), calculated dividing the conductance G_{Na} by the cell capacitance.

$$G_{Na} = G_{min} + \frac{(G_{max} - G_{min})}{\left[1+\exp\left[\frac{V - V_{1/2}}{dV}\right]\right]}$$

Equation (1) In Equation 1, G_{Na} is the Na^+ conductance at a given voltage V, G_{min}, and G_{max} are the conductance at the bottom and top plateaus, respectively; $V_{1/2}$ is the 50% of maximal conductance and dV is the slope of the curve between the two plateaus.

Western blot analysis

Brain tissue from male *Scn1a*$^{H939R/+}$ and male control mice (n = 3 per genotype) were lysed in radio-immunoprecipitation assay buffer containing 10 mg/ml each of aprotinin, phenylmethanesulfonyl fluoride and leupeptin (all from Sigma-Aldrich Canada, Oakville, ON, Canada) for 20 min at 4°, followed by centrifugation at 12,000 × g for 10 min. Total protein concentrations were determined by Bradford protein assay (Bio-Rad Laboratories, Hercules, CA). Protein samples were run on a 7.5% polyacrylamide gel, transferred onto a nitrocellulose membrane and incubated in blocking solution [Tris-buffered saline (TBS), 5% nonfat milk, 0.05% Tween-20] for 1 hr at room temperature followed by overnight incubation with primary $Na_v1.1$ polyclonal antibody (1:200; EMD Millipore, Burlington, MA) or βIII-tubulin (1:200; Abcam, Cambridge, UK) at 4°. Membranes were washed with TBS and 0.5% Tween-20 three times followed by incubation with secondary antibody (HRP-conjugated anti-rabbit or anti-mouse; Cell Signaling Technology, Danvers, MA) for 2 hr at room temperature. Blots were visualized by autoradiography using the Clarity Western ECL substrate (Bio-Rad Laboratories).

Immunohistochemistry (mouse brain hippocampal slice)

Under deep anesthesia, male 6-month-old mice (n = 3 per genotype) were injected transcardially, via the ascending aorta, with 15 ml of saline followed by 15 ml of fixative (4% paraformaldehyde, 0.2% picric acid in 0.1 M sodium phosphate buffer, pH 7.1). Following a 4 hr postfixation at 4°, the brain was transferred to 10% sucrose in 0.1 M sodium phosphate buffer, pH 7.1, for cryoprotection. Coronal cryostat sections of 12 μm were collected on gelatin-coated slides and stored at −80°.

Tissue sections were washed for a few minutes in 0.01 M phosphate-buffered saline (PBS). Sections were then incubated overnight at 4° with the primary antibody, diluted using 0.3% Triton X-100 in PBS. Primary antibodies were: vesicular acetylcholine transporter (vAChT, rabbit, 1:1000; SYnaptic SYstems, Goettengen, DE); parvalbumin (mouse, 1:4,000; Sigma-Aldrich Canada); nitric oxide synthase (NOS, rabbit, 1:200; Santa Cruz Biotechnology, Dallas TX); calretinin (goat, 1:400; Swant, Switzerland); or $Na_v1.1$ (rabbit, 1:1000; EMD Millipore).

After washing in PBS, sections were incubated with the appropriate conjugated Alexa Fluor secondary immunoglobulin (IgG) (dilution 1:400; Invitrogen, Carlsbad, CA) for 35 min at 37°. Sections washed in PBS were placed on coverslips using Fluoromount-G Anti-Fade (SouthernBiotech, Birmingham, AL).

Fluorescence staining was observed using a Zeiss Axioplan fluorescence microscope coupled to a Zeiss image analysis program, ZEN (Zeiss, Oberkochen, DE). Fluorescence values were quantified by ImageJ after the image was inverted and the background was eliminated by application of a small threshold. The threshold was user defined with reference to the original image and the same threshold value was maintained throughout all images analyzed. Fluorescence values were then compared between WT and *Scn1a*$^{H939R/+}$ mice by a two-way unpaired Student's t-test.

Immunocytochemistry (neuronal culture)

iPSC-derived iNPCs and iNs plated on glass cover slips (VWR, Randor, PA) were fixed for 15 min with 10% Formalin (Fisher Scientific, Hampton, NH) rinsed with 1× PBS (Wisent, Saint-Jean-Baptiste, QC, Canada) followed by permeabilization in 0.2%Tween-20/PBS (Sigma) for 10 min at room temperature. Following PBS rinse, serum-free protein blocking solution (Agilent, Santa Clara, CA) was applied for 1 hr. Primary antibodies were diluted in Antibody Diluent solution (Agilent) and iNs were incubated for 1 hr at room temperature. Antibodies used were Oct3/4 (1:100; Santa Cruz), Pax6 (1:100; Biolegend, San Diego, CA), Nanog (1:100; R&D Systems, Minneapolis, MN), Nestin (1:500; Millipore), Map2 (1:200; Sigma), NeuN (1:300; Millipore), GFAP (1:700; Agilent), βIII-tubulin (1:300; Millipore), Synaptophysin (1:00; Sigma), Synaptotagmin (1:100; Enzo Life Sciences, Farmingdale, NY), Gad 65+67

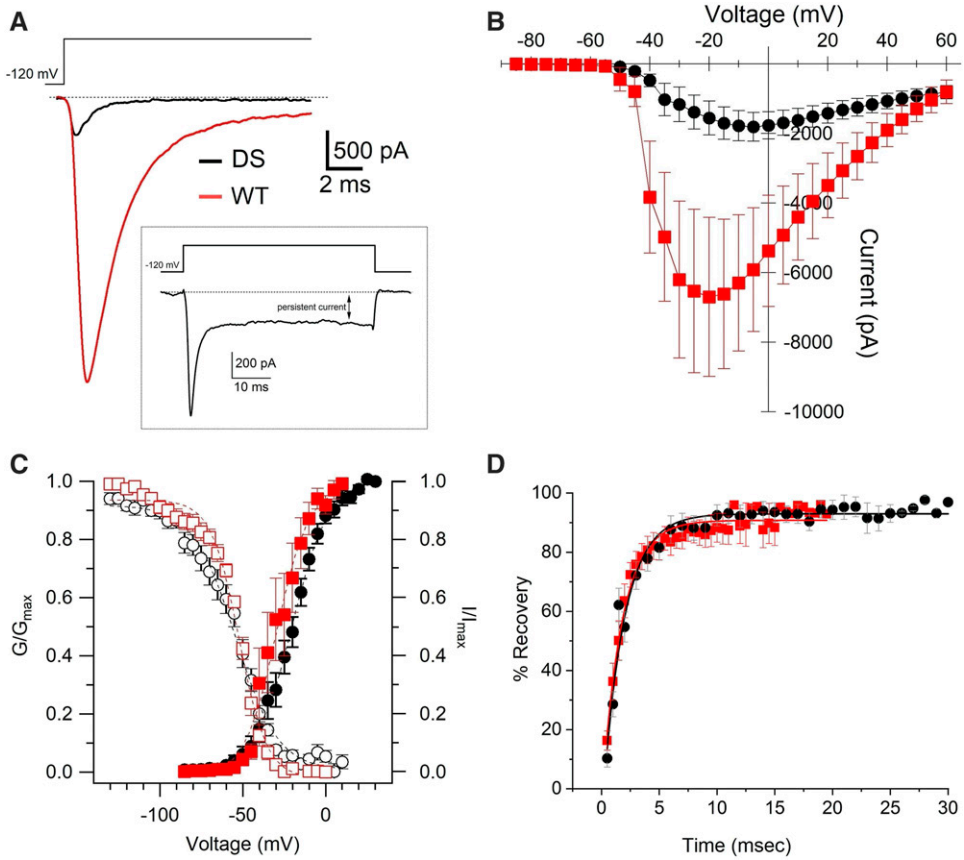

Figure 2 Characteristics of Na_v currents recorded in WT- and DS-iNs. (A) Example of peak Na_v currents recorded at −15 mV in WT- (red) and at −5 mV in DS- iNs (black). Inset. Example of Na_v persistent current recorded at 0 mV in a DS-iN. (B) Current voltage curves for WT- (red square, n = 8) and DS-iNs (black circle; n = 26). (C) Steady state inactivation (I/I_{max}; open symbols) and activation (G/G_{max}; full symbols) curves for WT- (red) and DS-iNs (black). (D) Recovery from inactivation curves for WT (red squares) and DS-iNs (black circles). For data summary see Table 1.

(1:100; Abcam), NMDAR1 (NR1, 1:100; Abcam), $GABA_A$ (1:100; Abcam). Subsequently, cover slips were rinsed with 1× PBS and secondary antibodies Goat anti-Rabbit Alexa Fluor 488, Donkey anti-Goat Alexa Fluor 488 or Goat anti-Mouse AlexaFluor568 (all 1:500; Life Technologies, Carlsbad, CA) were applied in 1× PBS for 1 hr at room temperature. Cover slips were rinsed in 1× PBS and were mounted using Dako Fluorescent Mounting Medium (Agilent) containing 2 μg/ml Hoechst33342 (Life Technologies). Images were acquired using Zeiss Axiovert 200 M fluorescence inverted microscope and Neofluar20×/0.50 Objective, analysis of images was done using AxioVision LE64 software.

Statistical analyses

All statistical analyses were performed using GraphPad Prism 5 or OriginPro 2017 software, with a P value < 0.05 considered statistically significant. Data values are expressed as mean ± SEM. Comparisons between datasets were made using a paired or unpaired Student's t-test; survival curves were created using the Kaplan–Meier method. One-way ANOVA with Bonferroni correction was applied to consider multiple comparisons in Figure 3.

Data availability

The mouse mutant *Scn1a*$^{H939R/+}$ described in this study is available from the Canadian Mouse Mutant Repository at The Centre for Phenogenomics (http://www.phenogenomics.ca). The authors state that all data necessary for confirming the conclusions presented in the article are represented fully within the article. Supplemental material available at figshare: https://doi.org/10.25386/genetics.12475901.

Results

Patient description

The patient was a 22-year-old female who had originally come to medical attention at 6 months of age with complex partial seizures following a febrile illness. Her seizure semiology evolved over time to include focal with or without secondary generalization, absence, tonic-clonic, and myoclonic seizures. She was clinically diagnosed with severe myoclonic epilepsy of infancy (Dravet syndrome) at 7 years of age and subsequently found to have a *de novo* pathogenic variant in *SCN1A*; c.2816A > G; p.His939Arg [NM_001165963.2]. Despite several medications (clobazam, valproate, stiripentol, ketogenic diet, cannabinoids at different combinations and dosages) she continues to have daily seizures and has intellectual disability and ataxia. Given the diagnosis of a rare syndrome, the patient and her parents were offered participation in the Care4Rare Canada Consortium, a research study that seeks to gain insights into the pathogenesis of rare diseases. Research ethics board approval was obtained, as was free and informed consent from the family prior to recruitment.

Table 2 Electrophysiological properties of WT- and DS-iNs

	WT-iNs	Ds-iNs
Resting membrane potential (mV)	−60.2 ± 3.7 (*n* = 6)	−47.2 ± 2.4* (*n* = 27)
Input resistance (MΩ)	1184 ± 341 (*n* = 6)	739.0 ± 125.6 (*n* = 27)
Spike threshold (mV)	−38.6 ± 0.91 (*n* = 6)	−38.9 ± 1.01 (*n* = 19)
Spike amplitude (mV)	79.07 ± 4.25 (*n* = 6)	62.31 ± 4.99* (*n* = 19)
Spike duration half amplitude (msec)	2.12 ± 0.25 (*n* = 6)	3.07 ± 0.36 (*n* = 19)
Slow I_{AHP} (mV)	16.63 ± 2.17 (*n* = 4)	8.64 ± 2.33 (*n* = 10)
Fast I_{AHP} (mV)	11.05 ± 1.83 (*n* = 5)	11.45 ± 2.57 (*n* = 8)
τ (at −20 pA)	131.95 ± 43.52 (*n* = 6)	38.12 ± 5.32 (*n* = 13)
Firing frequency (Hz)	13.2 ± 2.75 (*n* = 5)	14.36 ± 1.08 (*n* = 13)
Spiking pattern (%)		
No spike	0	29.6%
Single spike	0	7.4%
Repetitive	100	62.9%
Stuttering	0	7.4%

* $P < 0.05$.

Generation of patient-derived iPSCs and differentiation into neurons

An iPSC line was established from skin fibroblasts obtained from a biopsy specimen from the proband (DS-iPSC). Control experiments used the iPSC line, WT-iPSC, which was developed from human amniotic fluid cells as reported previously (Ribecco-Lutkiewicz *et al.* 2018). The iPSC colonies had typical human induced pluripotent stem cell morphology, with compact round colonies and high nuclear to cytoplasmic ratios (data not shown). During neural induction and neuronal differentiation, both DS-iPSC and WT-iPSC generated neural progenitor cells (iNPCs) expressing Pax6 and Nestin coincident with a loss of expression of pluripotency markers Oct 3/4 and Nanog (Figure 1, B and C). DS-iNPCs and WT-iNPCs were successfully differentiated toward mature neurons (iNs), as described in *Materials and Methods* and depicted in Figure 1, D and E. The DS-iN and WT-iNs showed characteristic neuronal morphology of defined cell bodies and branching neuronal networks structures as shown by Map2 and βIII-tubulin staining [Figure 1, D(i)–(iii) and E(i)]. The mature iNs expressed nuclear marker NeuN [Figure 1D(iii)], punctate synaptic protein expression of Synaptophysin, Synaptotagmin, synapsin, and GAD 65/67 [Figure 1, D(iv)–(vi) and E(ii)] and neuronal subtypes positive for GABA- A and NMDA (NR1) receptors [Figure 1D(vii), (viii)]. Heterogeneity of the neuronal cultures was further assessed by labeling for GFAP positive astrocytes [Figure 1, D(i) and 1E(iii)] that make up ∼10–20% of the cultures. The DS-iNs were also shown to express NOS, Parvalbumin, and Calretinin [Figure 1E(iv)–(vi)].

Electrophysiological characterization of Na_v currents in neurons (iNs) derived from fibroblasts of a DS patient with the pathogenic substitution, p.H939R

To characterize the effect of the pathogenic substitution p.H939R of a local DS patient, fibroblast cells from the proband (DS) were reprogrammed into induced pluripotent stem cells (DS-iPSCs) and then differentiated to neurons (DS-iNs) and compared alongside healthy WT-iNs. DS and WT-iNs were cultured and recorded in parallel to ensure the same degree of maturity. The Na_v currents from these iNs and WT controls were recorded using the patch-clamp whole-cell technique in voltage-clamp mode (see *Materials and Methods*). Table 1 shows a summary of the characteristics of the DS-iNs and WT-iNs Na_v currents. Significant differences were observed in peak current amplitude and activation kinetics (Figure 2 and Table 1). Na_v currents were significantly smaller in the DS-iNs (1997 ± 507 pA, $n = 26$) compared to WT-iNs (7516 ± 2199pA, $n = 8$; $P < 0.05$; see Figure 2, A and B and Table 1.) Activation kinetics (τ) were significantly slower in DS- (1.63 ± 0.38 ms, $n = 24$) than in WT-iNs (0.51 ± 0.11, $n = 7$; $P < 0.05$; Table 1). Finally, recovery from inactivation was not significantly different in the DS- (1.84 ± 0.16, $n = 18$) compared to WT-iNs (1.73 ± 0.12, $n = 7$; Figure 2D). In addition, 38.5% of the DS-iNs showed persistent currents (Figure 2A inset), while none were observed in WT-iNs. Another difference, although not statistically significant ($P = 0.08$), was observed in the voltage of the peak current (DS: 5.6 ± 2.8, $n = 26$; WT: −16.4 ± 5.2, $n = 7$). The Na^+ conductance was calculated as described in *Materials and Methods*. We found that the Na^+ conductance was lower in DS- (1.10 ± 0.22 nS/pF; $n = 26$) then in WT- (3.25 ± 1.19 nS/pF, $n = 7$) iNs.

Electro-responsive properties of the proband's iNs (DS-iNs)

To evaluate the effect of Na_v current differences between the DS-iNs and WT-iNs, we performed patch-clamp whole-cell recording in current-clamp mode. The electro-responsive properties of iNs were studied by applying current pulses from the resting membrane voltage (V_m); see *Materials and Methods*. Results are listed in Table 2. All WT-iNs showed repetitive spike trains that exhibited frequency adaptation when depolarized (Figure 3A). Interestingly, only 62.9% of the DS-iNs showed repetitive spikes trains and those were characterized by attenuating action potential amplitude (Figure 3B and Table 2). In addition, 7.4% DS-iNs showed a stuttering pattern, 7.4% a single spike and 29.6% no spiking activity at all (Table 2). We found that V_m was significantly more depolarized in the DS- (−47.2 ± 2.4 mV, $n = 27$) than in WT-iNs (−60.2 ± 3.7 mV,

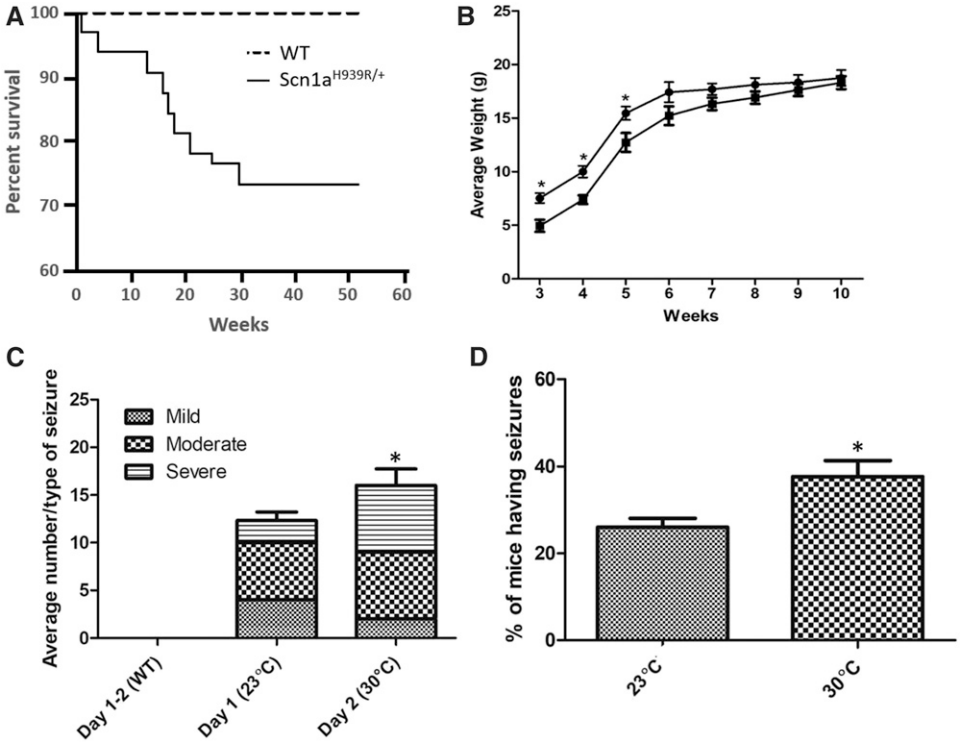

Figure 3 Physiological properties of the *Scn1a*$^{H939R/+}$ mice. (A) Survival curve. Male and female WT (dashed line; n = 40) and *Scn1a*$^{H939R/+}$ (solid line; n = 33) mice were monitored over 52 weeks. (B) Average weight over age (weeks) curve. Weekly measurements were taken over 10 weeks for WT (full circle; n = 10) and *Scn1a*$^{H939R/+}$ (full square; n = 10) mice. (C and D) Characterization of seizure activity. Seizures were monitored by video recording mice in phenotyping boxes for 2 days. Day 1 room temperature (23°) and day 2 30°. WT (n = 9) and *Scn1a*$^{H939R/+}$ (n = 10) mice were monitored at each temperature. (C) Average number of seizures at each temperature. Although there was not a significant increase in the number of seizures with temperature there was a significant difference in the number of "severe" seizures (horizontal lines) the mice experienced with increasing temperature. (D) Percent of *Scn1a*$^{H939R/+}$ mice having seizures at each temperature. *P = 0.05. Note that WT mice do not have seizures at any temperature tested.

$n = 6$; $P < 0.05$). The action potential (spike) amplitude of the DS-iNs was also significantly smaller (62.31 ± 4.99 mV, $n = 19$; only the first and largest action potential was considered for this measure) compared to WT-iNs (79.07 ± 4.25 mV, $n = 6$; $P < 0.05$), while input resistance (R_{in}), spike threshold, spike duration at half amplitude, slow after-hyperpolarization (I_{AHP}), fast I_{AHP}, τ, and firing frequency (see *Materials and Methods*) were not significantly different (Table 2). These results suggest that the p.H939R substitution in the $Na_v1.1$ channel causes changes in the electro-responsive properties of neurons expressing the impaired channel.

Characterization of the Scn1a$^{H939R/+}$ mouse model based on the patient $Na_v1.1$ substitution p.H939R

The *Scn1a*$^{H939R/+}$ mice showed increased mortality compared to their WT littermates, with 25% demise by 30 weeks of age (Figure 3A). Upon weaning at 3 weeks, heterozygous mice were smaller than their WT littermates. This difference disappeared by 10 weeks of age (Figure 3B). The mice also showed spontaneous seizure activity that consisted of myoclonic jerks, as well as repetitive flexion/extension of limbs followed by up to 1 min of immobility). A total of 9 WT and 10 *Scn1a*$^{H939R/+}$ mice were assessed at 23° and 30° (Figure 3, C and D). Increasing the ambient temperature increased seizure frequency in *Scn1a*$^{H939R/+}$ mice, and is consistent with the DS phenotype.

Electrophysiological characterization of pyramidal neurons and interneurons of the CA1 region of the hippocampus in Scn1a$^{H939R/+}$ mice

To gain insight into the neuronal network make-up causing seizures in *Scn1a*$^{H939R/+}$ mice, we studied the electrophysiological properties of pyramidal neurons and interneurons of the CA1 region of the hippocampus and compared them with that of WT mice, using whole-cell patch-clamp recording in brain slices. The electro-responsive properties of pyramidal neurons (WT, $n = 23$; *Scn1a*$^{H939R/+}$, $n = 15$) and interneurons (WT, $n = 46$; *Scn1a*$^{H939R/+}$, $n = 42$) were studied in current-clamp by applying 500 msec current pulses from V_m in ACSF (see *Materials and Methods*). Cells were visually identified in hippocampal slices with IR-DIC and selected for recordings on the basis of their morphology and localization in specific layers of the CA1 region (see *Materials and Methods*). Pyramidal neurons and interneurons were recorded in the pyramidal layer and stratum radiatum, respectively. In both WT and *Scn1a*$^{H939R/+}$ mice, the interneurons sustained high firing rates without or with various degrees of accommodation (Figure 4, C and D) while the pyramidal neurons generated spike trains that exhibited frequency adaptation when depolarized (Figure 4F). A summary of the electrophysiological properties of the pyramidal neurons and interneurons recorded in this study is provided in Table 3. We found that V_m was significantly more depolarized in both pyramidal neurons and interneurons in *Scn1a*$^{H939R/+}$ (pyramidal neurons, −60.9 ± 1.46 mV, $P < 0.005$; interneurons, −47.02 ± 0.82 mV, $P < 0.05$) than in their WT littermates (pyramidal neurons, −68.17 ± 0.7 mV; interneurons, −49.67 ± 0.84 mV). In addition, the firing frequency of interneurons (Figure 4B) in *Scn1a*$^{H939R/+}$ (15.7 ± 1.94 Hz), was significantly lower than in WT (20.6 ± 1.25 Hz), while unchanged in pyramidal neurons in both *Scn1a*$^{H939R/+}$and WT mice (Figure 4E). The percentage of interneurons with fast spiking and stuttering firing pattern was

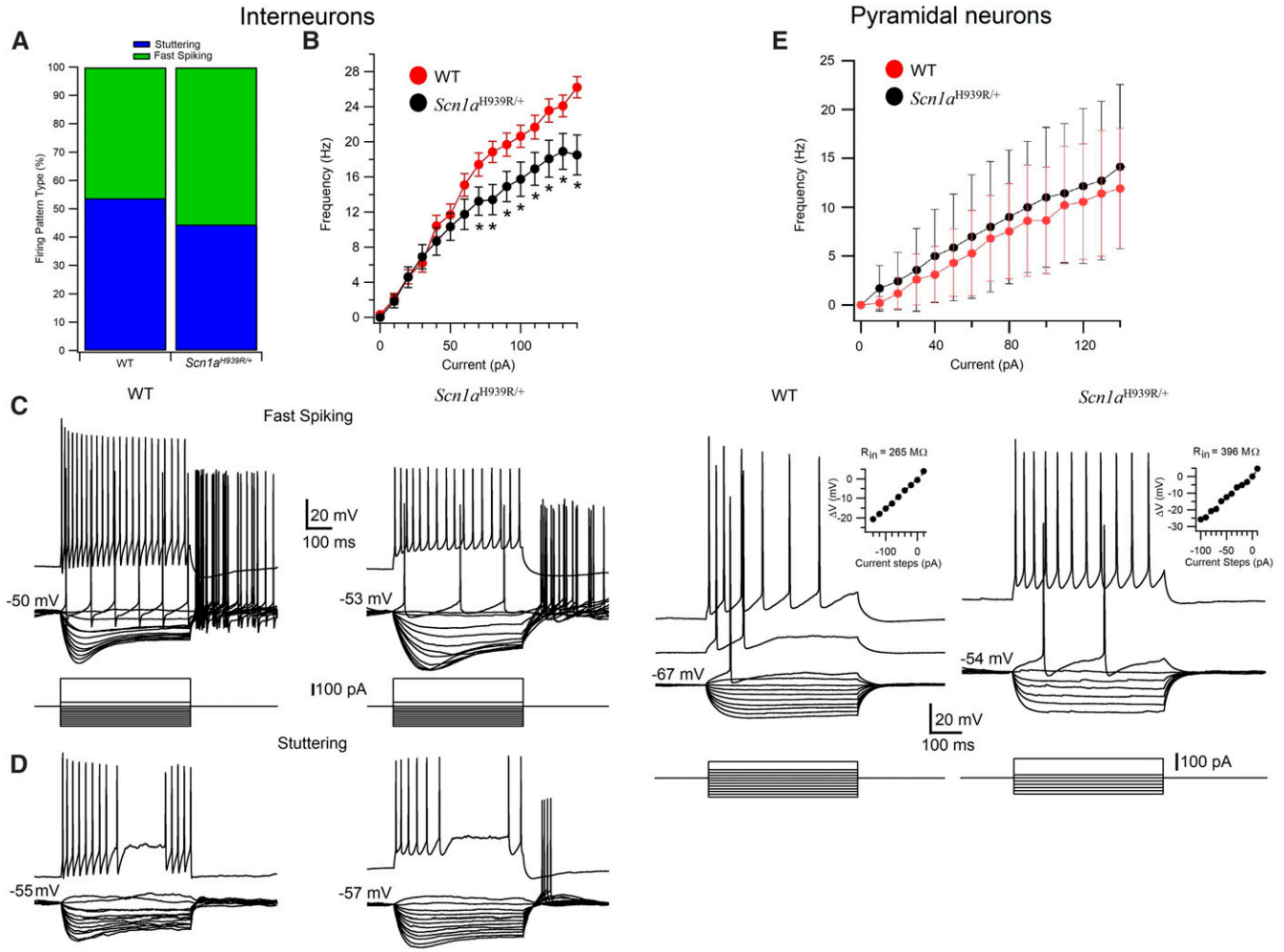

Figure 4 Electrophysiological properties of interneurons (A–D) and pyramidal neurons (E and F) recorded in the stratum radiatum and stratum pyramidale of the CA1 region of the hippocampus in WT and *Scn1a*$^{H939R/+}$ mice. (A) Percentage of interneurons with stuttering and fast-spiking firing patterns in WT and *Scn1a*$^{H939R/+}$ mice. (B) Frequency of action potentials in interneurons as a function of the injection of incremental steps of current in WT (red dots) and *Scn1a*$^{H939R/+}$ (black dots) mice. (C and D) Voltage responses of interneurons with different firing pattern (fast spiking, top; stuttering, bottom) recorded in WT (left) and *Scn1a*$^{H939R/+}$ (right) mice, to a series of intracellular current pulses (C bottom traces). The current steps were applied at voltage membrane resting potentials. (E) Frequency of action potentials in pyramidal neurons as a function of the injection of incremental steps of current in WT (red dots) and *Scn1a*$^{H939R/+}$ (black dots) mice. (F) Voltage responses of pyramidal neurons recorded in WT (left) and *Scn1a*$^{H939R/+}$ (right) mice, to a series of intracellular current pulses (bottom). The current steps were applied at rest. Insets: voltage-current curves.

slightly but not significantly different ($P = 0.44$; chi-squared test) in *Scn1a*$^{H939R/+}$ (45% stuttering and 55% fast spiking) and WT mice (54% stuttering and 46% fast spiking) (Figure 5A). The action potential (spike) threshold was significantly more depolarized in the interneurons of WT (-40.54 ± 0.71 mV, $n = 46$) compared to *Scn1a*$^{H939R/+}$ (-42.42 ± 0.20 mV, $n = 42$) mice, while unchanged in pyramidal cells of both types of mice (Table 3). The action potential amplitude of pyramidal neurons was also significantly smaller in *Scn1a*$^{H939R/+}$ (99.1 ± 2.5 mV) compared to WT (104.8 ± 0.83 mV; $P < 0.05$), while R_{in}, spike duration at half amplitude, slow I_{AHP}, fast I_{AHP}, and τ (see *Materials and Methods*) were similar (Table 3). These data, except for the Spike threshold, are consistent with those observed in DS-iNs described above.

Overall, these results underline a hyper-excitability of the CA1 circuit, which, under certain conditions such as temperature, can trigger seizures.

Level of Na_v 1.1 protein expression in the hippocampus of Scn1a$^{H939R/+}$ mouse

Western blot and immunofluorescence experiments were performed to evaluate the level of $Na_v1.1$ protein expression. No difference in localization, size or expression of the $Na_v1.1$ protein was observed in the *Scn1a*$^{H939R/+}$ mouse brain compared to controls (Figure S1, A and B). These data, together with the characterization of Na_v current (Figure 2, A and B and Table 1) are consistent with a lower Na^+ conductance when the p.H939R mutation is present despite the equal number of channels expressed in WT and *Scn1a*$^{H939R/+}$ mice.

Table 3 Electrophysiological properties of pyramidal neurons and interneurons recorded in the CA1 region of the hippocampus in WT and *Scn1a*$^{H939R/+}$ mice

	Pyramidal neurons		Interneurons	
	WT (n = 23)	*Scn1a*$^{H939R/+}$ (n = 15)	WT (n = 46)	*Scn1a*$^{H939R/+}$ (n = 42)
Resting membrane potential (mV)	−68.17 ± 0.7	−60.9 ± 1.46**	−49.67 ± 0.84	−47.02 ± 0.82*
Input resistance (MΩ)	509 ± 23	481 ± 27	311.8 ± 20.16	306.1 ± 17.03
Spike threshold (mV)	−47.5 ± 0.63	−46.63 ± 0.99	−40.54 ± 0.71	−42.42 ± 0.20*
Spike amplitude (mV)	104.8 ± 0.83	99.1 ± 2.5*	78.06 ± 1.63	77.20 ± 1.58
Spike duration half amplitude (msec)	1.84 ± 0.06	1.78 ± 0.04	1.36 ± 0.06	1.32 ± 0.05
Slow I_{AHP} (mV)	5.23 ± 0.53	6.73 ± 1.07	11.59 ± 0.81	12.17 ± 0.83
Fast I_{AHP} (mV)	4.42 ± 0.61	5.09 ± 0.81	12.21 ± 0.90	10.17 ± 0.83
τ (at −100 pA)	28.12 ± 1.82	26.4 ± 3.81	31.20 ± 1.89	30.74 ± 1.99
Firing frequency, 100 pA step at −60 mV (Hz)	8.64 ± 5.46	11 ± 7.14	20.6 ± 1.25	15.7 ± 1.94*

* $p < 0.05$, ** $P < 0.005$.

Reduction of interneuron markers in the CA1 region of the Scn1a$^{H939R/+}$ hippocampus

To gain insight into the mechanism underlining the hyper-excitability of the CA1 circuit of the *Scn1a*$^{H939R/+}$ mouse hippocampus, immunohistochemical analysis was made using interneuron markers. Reductions in the expression of vesicular acetylcholine transporter (vAChT), parvalbumin (ParV) and nitric oxide synthase (NOS) were observed in the *Scn1a*$^{H939R/+}$ compared to WT mice (Figure 5). There were no measurable differences in calretinin or tyrosine hydroxylase (data not shown). These findings are in alignment with other reports showing reduced parvalbumin expression in DS mouse models (Yu *et al.* 2006). Interestingly, also the neuronal nitric oxide synthase (nNOS)-expressing cells, which constitute a large GABAergic interneuron population in the hippocampus, seemed to be reduced. This could suggest a reduction in the overall population of interneurons. In addition, the reduction in vAChT suggests a potential involvement of the cholinergic system in DS pathology.

Discussion

We have generated a novel DS mouse model (*Scn1a*$^{H939R/+}$) and iPSC line based on an amino acid substitution (p.H939R) in the $Na_v1.1$ channel, modeled on a local individual with DS. We found a hyper-excitability of the CA1 circuit which, under certain conditions such as temperature, can trigger seizures. We suggest that this hyper-excitability is due to the altered electrophysiological properties of interneurons and the pyramidal cells deriving from the dysfunction of the $Na_v1.1$ channel bearing the p.H939R substitution. These results are supported by DS-iNs data showing the same electrophysiological phenotype as observed in the *Scn1a*$^{H939R/+}$ hippocampal neurons.

The characterization of the $Na_v1.1$ channel properties—showing smaller currents in DS-iNs—together with data from the $Na_v1.1$ protein level analysis in *Scn1a*$^{H939R/+}$ mouse brain—showing no alteration in localization, size, or expression of the $Na_v1.1$ protein compared to WT—suggest a lower sodium conductance when the p.H939R mutation is present, despite the equal number of channels expressed in WT and *Scn1a*$^{H939R/+}$ mice. In addition, the immunohistochemical studies of interneuron markers suggest a reduction in the overall population of interneurons and a potential involvement of the cholinergic system in DS pathology.

Several mouse models now exist for DS that point to dysfunctional interneurons as responsible for the disease phenotype (Catterall 2018). The genetic models to date comprise (i) *Scn1a* deletions (first and last exons), (ii) a nonsense mutation (Yu *et al.* 2006; Ogiwara *et al.* 2007; Miller *et al.* 2014), (iii) a recent missense variant (Ricobaraza *et al.* 2019), and (iv) conditional *Scn1a* haploinsufficiency mutants expressed in specific neuronal subtypes (Cheah *et al.* 2012; Dutton *et al.* 2013; Ogiwara *et al.* 2013; Rubinstein, *et al.* 2015; Tatsukawa *et al.* 2018). While the haploinsufficiency of $Na_v1.1$ in the cortical interneurons is sufficient to cause a Dravet-phenotype (Cheah *et al.* 2012), the different models show subtle phenotypic differences. The mortality rate, frequency, and types of seizures, in addition to the extent of cognitive deficits and other behavioral comorbidities, vary in frequency given mouse age, background strain, and the environmental trigger.(Ito *et al.* 2013; Mistry *et al.* 2014; Favero *et al.* 2018; Rubinstein *et al.* 2015a,b; Ricobaraza *et al.* 2019)

When *Scn1a* haploinsufficiency is expressed in parvalbumin- or somatostatin-expressing interneurons, differing behavioral phenotypes (autism-like, hyperactivity) can be observed (Rubinstein *et al.* 2015a). In the models studied to date, pyramidal cells have largely shown no difference in their excitability compared to controls. The only exception is a study of dissociated neurons from the hippocampus of a *Scn1a* haploinsufficient mouse (exon one deletion) that showed increased sodium channel density, spontaneous firing, and sustained firing of pyramidal cells at day 21–24 of age (Mistry *et al.* 2014). The previous *Scn1a* haploinsuffiency mouse models had been studied at a younger age (Yu *et al.* 2006; Ogiwara *et al.* 2007). Similarly, the work presented here shows that not only can the interneuron be predominantly impacted by the p.H939R substitution, but also the pyramidal neuron of the hippocampus can be altered. The whole-cell patch-clamp studies of the hippocampus showed

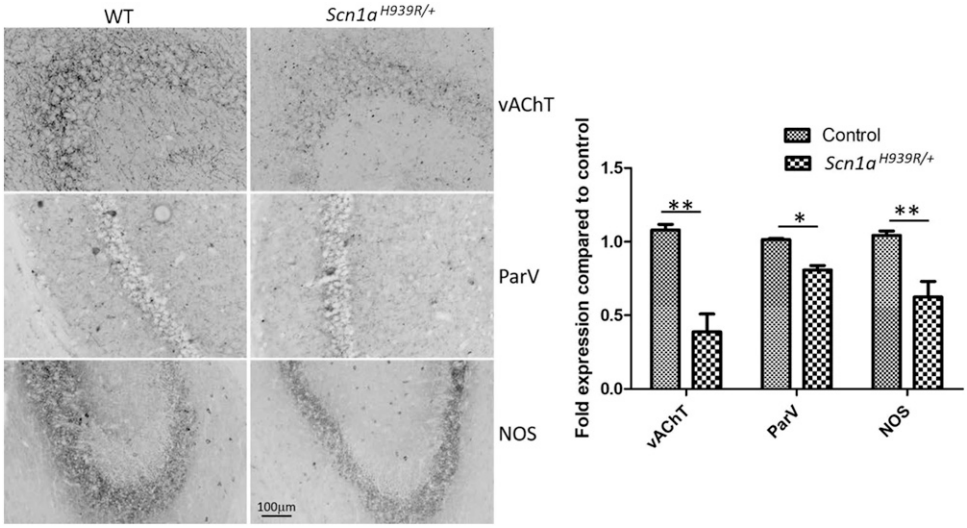

Figure 5 Reduction in immunohistochemical markers for interneurons in the hippocampus of the *Scn1a*$^{H939R/+}$ compared to WT mice. Inverted immunostaining of vAChT-, ParV-, and NOS-positive interneurons. Mice (n = 3) were 6 months old at time of immunostaining. *$P < 0.05$, **$P < 0.01$.

a consistently depolarized resting membrane potential and differences in the overall spike amplitude of the pyramidal cells. This shows the contribution of both cell types to network excitability and promotion of seizure activity in 8-week-old mice. These results were supported by the data obtained in DS- and WT-iNs showing similar difference in V_m and spike amplitude.

Pyramidal cells have been implicated previously in *in vitro* model systems involving induced neurons (Liu *et al.* 2013). Fibroblasts from individuals with DS were reprogrammed into pyramidal cells and interneurons, and both induced cell types showed differences in sodium channel densities, thresholds for action potential generation, and increased repetitive firing frequency (Liu *et al.* 2013). Differences were observed in the resting membrane potentials of both types of induced neurons (Liu *et al.* 2013). To characterize the pathogenic substitution p.H939R, fibroblasts from the proband were reprogrammed into iPSCs and then differentiated to mixed forebrain iNs. We cannot distinguish between excitatory or inhibitory neurons in the population of iNs we recorded. Consequently, the difference in the electro-responsive properties we measured may be underestimated, due to the presence of excitatory neurons that have been described to be similar between WT and DS.

A novel finding in this mouse model is the decreased expression of various markers for the interneurons of the hippocampus including parvalbumin and vesicular acetylcholine transferase. Reduced parvalbumin is consistent with previous reports (Tai *et al.* 2014). Reduction in acetylcholine, however, has not been reported previously but is consistent with recent work showing the protective effect of acetylcholine esterase inhibitors (huperzine A, donepezil) on induced seizures in a haploinsufficiency model (Wong *et al.* 2016, 2019). In addition, reduction in acetylcholine would lead to hippocampal excitation as this neurotransmitter normally binds to muscarinic receptors on GABAergic interneurons inhibiting the excitatory pyramidal neurons.

The variability observed in the mouse models response to treatment (Hawkins *et al.* 2017) is in keeping with the experience of individuals with DS (Wirrell 2016). Treatment regimens typically evolve with respect to the specific medication, the dosages and the combinations over the course of a patient's life. Given this variability, having a broad array of tools, including several model systems (iPSCs, zebrafish, mice, *Drosophila*) that can represent the underlying disease process, will be valuable for those pursuing drug screening or detailed preclinical studies. Already, information regarding the underlying pathogenesis of DS has provided targeted strategies for preclinical therapy. Interneuron function has been successfully restored with a dCas9-Scn1a vector (Colasante *et al.* 2020) and with snake venom (Richards *et al.* 2018) in the haploinsufficiency mouse models. A sodium channel modulator (GS967) was also shown to suppress the aberrant firing of pyramidal cells in older mice (Anderson *et al.* 2017). We hypothesize that the varieties (strain, age, and genotype) of DS will each have unique contributions of neuronal cell types and that models that incorporate these differences will be beneficial tools to develop new treatments and insights into disease pathogenesis.

Acknowledgments

We would like to acknowledge the generosity of the family for participating in this research. We are thankful for the work performed by the Behaviour and Physiology Core at the University of Ottawa. We would also like to acknowledge the helpful discussion with Peter Juranka, and Caroline Sodja for her help in making the schematic in Figure 1. Funding for the generation and phenotyping of this mouse model was provided by the Ontario Brain Institute (Eplink), the Rare Diseases: Models and Mechanisms Network (RDMM), and Dravet.ca. In addition, Genome Canada and Ontario Genomics (OGI-051) funded the NorCOMM2 project that supported production of the mutant allele. Research

in collaboration with National Research Council of Canada (NRC) was funded by the NRC New Beginnings/Ideation Fund. The authors have no competing interests to declare.

Literature Cited

Anderson, L. L., N. A. Hawkins, C. H. Thompson, J. A. Kearney, and A. L. George, 2017 Unexpected efficacy of a novel sodium channel modulator in Dravet syndrome. Sci. Rep. 7: 1682. https://doi.org/10.1038/s41598-017-01851-9

Catterall, W. A., 2018 Dravet syndrome: a sodium channel interneuronopathy. Curr. Opin. Physiol. 2: 42–50. https://doi.org/10.1016/j.cophys.2017.12.007

Cheah, C. S., F. H. Yu, R. E. Westenbroek, F. K. Kalume, J. C. Oakley *et al.*, 2012 Specific deletion of NaV1.1 sodium channels in inhibitory interneurons causes seizures and premature death in a mouse model of Dravet syndrome. Proc. Natl. Acad. Sci. USA 109: 14646–14651. https://doi.org/10.1073/pnas.1211591109

Claes, L., J. Del-Favero, B. Ceulemans, L. Lagae, C. Van Broeckhoven *et al.*, 2001 De novo mutations in the sodium-channel gene SCN1A cause severe myoclonic epilepsy of infancy. Am. J. Hum. Genet. 68: 1327–1332. https://doi.org/10.1086/320609

Colasante, G., G. Lignani, S. Brusco, C. Di Berardino, J. Carpenter *et al.*, 2020 dCas9-based Scn1a gene activation restores inhibitory interneuron excitability and attenuates seizures in Dravet syndrome mice. Mol Ther. 28: 235–253. https://doi.org/10.1016/j.ymthe.2019.08.018

Dravet, C., 2011 The core Dravet syndrome phenotype. Epilepsia 52: 3–9. https://doi.org/10.1111/j.1528-1167.2011.02994.x

Dutton, S. B., C. D. Makinson, L. A. Papale, A. Shankar, B. Balakrishnan *et al.*, 2013 Preferential inactivation of Scn1a in parvalbumin interneurons increases seizure susceptibility. Neurobiol. Dis. 49: 211–220. https://doi.org/10.1016/j.nbd.2012.08.012

Favero, M., N. P. Sotuyo, E. Lopez, J. A. Kearney, and E. M. Goldberg, 2018 A transient developmental window of fast-spiking interneuron dysfunction in a mouse model of Dravet syndrome. J. Neurosci. 38: 7912–7927. https://doi.org/10.1523/JNEUROSCI.0193-18.2018

Gertsenstein, M., and L. M. J. Nutter, 2018 Engineering point mutant and epitope-tagged alleles in mice using Cas9 RNA-guided nuclease. Curr. Protoc. Mouse Biol. 8: 28–53. https://doi.org/10.1002/cpmo.40

Hawkins, N. A., L. L. Anderson, T. S. Gertler, L. Laux, A. L. George *et al.*, 2017 Screening of conventional anticonvulsants in a genetic mouse model of epilepsy. Ann. Clin. Transl. Neurol. 4: 326–339. https://doi.org/10.1002/acn3.413

Hirose, S., I. E. Scheffer, C. Marini, P. De Jonghe, E. Andermann *et al.*, 2013 SCN1A testing for epilepsy: application in clinical practice. Epilepsia 54: 946–952. https://doi.org/10.1111/epi.12168

Ito, S., I. Ogiwara, K. Yamada, H. Miyamoto, T. K. Hensch *et al.*, 2013 Mouse with Nav1.1 haploinsufficiency, a model for Dravet syndrome, exhibits lowered sociability and learning impairment. Neurobiol. Dis. 49: 29–40. https://doi.org/10.1016/j.nbd.2012.08.003

Klausberger, T., 2009 GABAergic interneurons targeting dendrites of pyramidal cells in the CA1 area of the hippocampus. Eur. J. Neurosci. 30: 947–957. https://doi.org/10.1111/j.1460-9568.2009.06913.x

Klausberger, T., L. F. Marton, J. O'Neill, J. H. Huck, Y. Dalezios *et al.*, 2005 Complementary roles of cholecystokinin- and parvalbumin-expressing GABAergic neurons in hippocampal network oscillations. J. Neurosci. 25: 9782–9793. https://doi.org/10.1523/JNEUROSCI.3269-05.2005

Liu, Y., L. F. Lopez-Santiago, Y. Yuan, J. M. Jones, H. O. Zhang, *et al.*, 2013 Dravet syndrome patient-derived neurons suggest a novel epilepsy mechanism. Ann. Neurol. 74: 128–139. https://doi.org/10.1002/ana.23897

Miller, A. R., N. A. Hawkins, C. E. McCollom, and J. A. Kearney, 2014 Mapping genetic modifiers of survival in a mouse model of Dravet syndrome. Genes Brain Behav. 13: 163–172. https://doi.org/10.1111/gbb.12099

Mistry, A. M., C. H. Thompson, A. R. Miller, C. G. Vanoye, A. L. George *et al.*, 2014 Strain- and age-dependent hippocampal neuron sodium currents correlate with epilepsy severity in Dravet syndrome mice. Neurobiol. Dis. 65: 1–11. https://doi.org/10.1016/j.nbd.2014.01.006

Oakley, J. C., F. Kalume, and W. A. Catterall, 2011 Insights into pathophysiology and therapy from a mouse model of Dravet syndrome. Epilepsia 52: 59–61. https://doi.org/10.1111/j.1528-1167.2011.03004.x

Ogiwara, I., H. Miyamoto, N. Morita, N. Atapour, E. Mazaki *et al.*, 2007 Nav1.1 localizes to axons of parvalbumin-positive inhibitory interneurons: a circuit basis for epileptic seizures in mice carrying an Scn1a gene mutation. J. Neurosci. 27: 5903–5914. https://doi.org/10.1523/JNEUROSCI.5270-06.2007

Ogiwara, I., T. Iwasato, H. Miyamoto, R. Iwata, T. Yamagata *et al.*, 2013 Nav1.1 haploinsufficiency in excitatory neurons ameliorates seizure-associated sudden death in a mouse model of Dravet syndrome. Hum. Mol. Genet. 22: 4784–4804. https://doi.org/10.1093/hmg/ddt331

Ribecco-Lutkiewicz, M., C. Sodja, J. Haukenfrers, A. S. Haqqani, D. Ly *et al.*, 2018 A novel human induced pluripotent stem cell blood-brain barrier model: applicability to study antibody-triggered receptor-mediated transcytosis. Sci. Rep. 8: 1873. https://doi.org/10.1038/s41598-018-19522-8

Richards, K. L., C. J. Milligan, R. J. Richardson, N. Jancovski, and M. Grunnet, 2018 Selective $Na_V1.1$ activation rescues Dravet syndrome mice from seizures and premature death. Proc. Natl. Acad. Sci. USA 115: E8077–E8085. https://doi.org/10.1073/pnas.1804764115

Ricobaraza, A., L. Mora-Jimenez, E. Puerta, R. Sanchez-Carpintero, A. Mingorance *et al.*, 2019 Epilepsy and neuropsychiatric comorbidities in mice carrying a recurrent Dravet syndrome SCN1A missense mutation. Sci. Rep. 9: 14172. https://doi.org/10.1038/s41598-019-50627-w

Rubinstein, M., S. Han, C. Tai, R. E. Westenbroek, A. Hunker *et al.*, 2015a Dissecting the phenotypes of Dravet syndrome by gene deletion. Brain 138: 2219–2233. https://doi.org/10.1093/brain/awv142

Rubinstein, M., R. E. Westenbroek, F. H. Yu, C. J. Jones, T. Scheuer *et al.*, 2015b Genetic background modulates impaired excitability of inhibitory neurons in a mouse model of Dravet syndrome. Neurobiol. Dis. 73: 106–117. https://doi.org/10.1016/j.nbd.2014.09.017

Tai, C., Y. Abe, R. E. Westenbroek, T. Scheuer, and W. A. Catterall, 2014 Impaired excitability of somatostatin- and parvalbumin-expressing cortical interneurons in a mouse model of Dravet syndrome. Proc. Natl. Acad. Sci. USA 111: E3139–E3148. https://doi.org/10.1073/pnas.1411131111

Tatsukawa, T., I. Ogiwara, E. Mazaki, A. Shimohata, and K. Yamakawa, 2018 Impairments in social novelty recognition and spatial memory in mice with conditional deletion of Scn1a in parvalbumin-expressing cells. Neurobiol. Dis. 112: 24–34. https://doi.org/10.1016/j.nbd.2018.01.009

Wirrell, E. C., 2016 Treatment of Dravet syndrome. Can. J. Neurol. Sci. 43: S13–S18. https://doi.org/10.1017/cjn.2016.249

Wong, J. C., S. B. Dutton, S. D. Collins, S. Schachter, and A. Escayg, 2016 Huperzine A provides robust and sustained protection against induced seizures in. Front. Pharmacol. 7: 357. https://doi.org/10.3389/fphar.2016.00357

Wong, J. C., J. T. Thelin, and A. Escayg, 2019 Donepezil increases resistance to induced seizures in a mouse model of Dravet syndrome. Ann. Clin. Transl. Neurol. 6: 1566–1571.

Yu, F. H., M. Mantegazza, R. E. Westenbroek, C. A. Robbins, F. Kalume, *et al.*, 2006 Reduced sodium current in GABAergic interneurons in a mouse model of severe myoclonic epilepsy in infancy. Nat. Neurosci. 9: 1142–1149. https://doi.org/10.1038/nn1754

Communicating editor: J. Schimenti